Improving OPC Model Accuracy of Dry Resist for Low k1 EUV Patterning

Dongbo Xu[a], Werner Gillijns[b], Stewart Wu[a], Shruti Jambaldinni[c], Benjamin Kam[c], Anuja De Silva[c], and Germain Fenger[d]

[a]Siemens EDA, Belgium
[b]imec, Belgium
[c]Lam Research Belgium BV, Belgium
[d]Siemens EDA, United States

ABSTRACT

Extreme ultraviolet lithography (EUVL) with a numerical aperture of 0.33 has been part of high-volume manufacturing since 2019. To guarantee the downscaling of the technology node, advanced material and patterning becomes very critical in terms of resolution, roughness, defectivity and process window. Therefore, several entities are developing new resists and processes. However, to adopt new resist and process into production, performing model-based optical proximity correct (OPC) is an essential step. Thus, an accurate OPC model is required. In this paper, we investigate the Siemens calibre CM1 OPC model accuracy of dry resist process, which is conducted on N5 M2 design (horizontal pitch 32nm).

Keywords: EUV Single Patterning, Dry Resist, Model Accuracy, OPC Model

1. INTRODUCTION

EUV Lithography (EUVL) with a numerical aperture (NA) of 0.33 is the key to advance Moore's Law by driving the semiconductor devices to smaller dimensions. Nowadays, EUVL patterning has been successfully adopted in high-volume manufacturing (HVM) to further reduce the cost at advanced nodes. However, the occurrence of stochastic printing failures in EUVL patterning is critical at tight pitches.[1–4] To guarantee the downscaling of the technology node, photoresist is a critical element to sustain the lithographic patterning performance in terms of yield, resolution, defectivity free, and process window. As the 0.55NA EUVL approaches its insertion point in the HVM, the focus on the readiness of the required photoresist further intensifies. However, due to the triangle trade-off relationship among resolution, line-edge roughness (LER) and dose/sensitivity (RLS),[5–7] there are contradictory requirements for a resist to have low LER, high dose sensitivity and high resolution simultaneously.

The dry resist provides a simple, homogeneous, and stable composition of metal oxide network after deposition, EUV exposure, post-exposure bake, which breaks several long standing tradeoffs in EUV photoresist materials.[8] It allows to tune the conditions during the pattern development process to provide optimum dry photoresist integrity, to improve pattern fidelity and overall defectivity, and shows promising patterning performance towards 0.55NA EUVL.[9,10] To adopt this new resist and process into production of advanced node, only full model-based optical proximity correct (OPC) solutions can meet the required accuracy to control the edge placement errors. Thus, calibrating an accurate OPC model is an essential step. To quantify Siemens calibre CM1 OPC model accuracy of dry resist process, an imec Ta-based dark field EUV mask was used. Since the dry resist is a negative-tone resist, the designed polygon on the mask (mask mirror) is printed as resist line on the wafer. The imec horizontal pitch 32nm M2 design (N5) was selected as the target layer, and the wafer data was exposed by using imec NXE:3400 EUV scanner and HITACHI CD-SEM was used for images acquisition.

The paper is organized as follows: Section 2 introduces feature selection and OPC model calibration strategy. The model accuracy and patterning challenges of dry resist process will be investigated in Section 3. The last section will provide the summary.

Dongbo Xu: dongbo.xu@siemens.com

2. MODEL ACCURACY STUDY STRATEGY

In this paper, OPC model accuracy study is conducted on imec horizontal pitch 32nm (N5) M2 design. Figure 1 shows the selected features based on the design rule, which includes:

- One Dimension (1D) features: (Line/Space(LS) without SRAF (sub-resolution assist feature): LS with SRAF, Two-Bar without SRAF, Two-Bar with SRAF, multiple-Bar(M-Bar) without SRAF, M-Bar with SRAF.
- One and a half Dimension (1.5D) features: tip-to-tip (T2T), multiple-T2T (M-T2T).
- Two Dimension (2D) features: different types of contact holes (CH), TShape, uDBCD and so on.
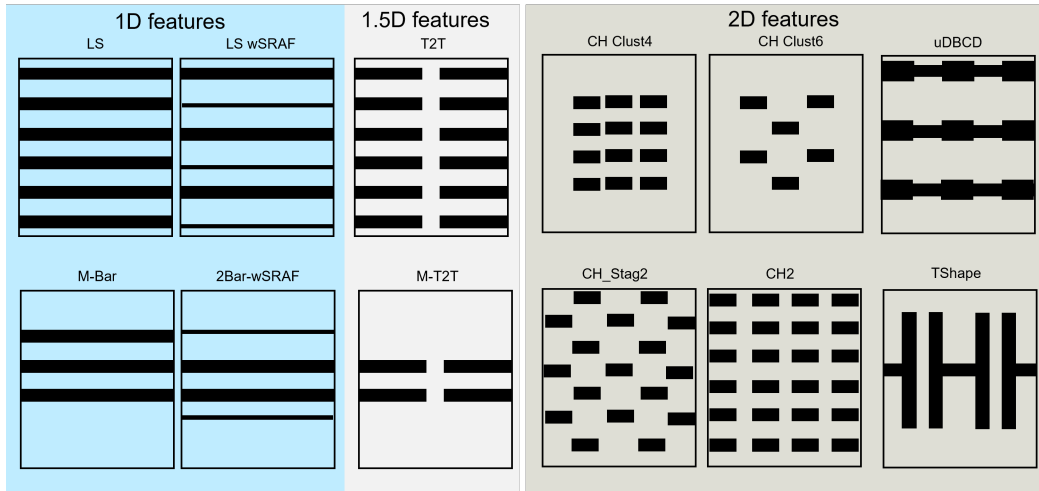

Figure 1: Selected features based on the design rule, which includes 1D features ((Line/Space(LS) without SRAF, LS with SRAF, Two-Bar without SRAF, Two-Bar with SRAF, multiple-Bar(M-Bar) without SRAF, M-Bar with SRAF), 1.5D features (tip-to-tip (T2T), multiple-T2T(M-T2T)) and 2D features (different types of contact holes (CH), TShape, uDBCD and so on).

Figure 2 illuminates the OPC modeling accuracy strategy. To calibrate an accurate OPC model, we need to have a good understanding about the process; thus, the OPC model accuracy study on dry resist is carried out into two parts: model calibration based on features without SRAFs, and model calibration by using features without and with SRAFs. To simplify our study in this paper, we are focusing on 1D and 1.5D features without SRAFs by using CD gauges, the main goal is to understand the dry resist process and to verify calibre CM1 model terms. Therefore, we will not discuss advanced model calibration (such as contour-based modeling, SRAF printing model, stochastic modeling) in this paper.

3. MODEL ACCURACY AND PATTERNING CHALLENGES

To study the new dry resist process, imec Process of Reference (PoR) chemical amplified resist (CAR) process has been chosen as the reference process, and the Titan M2 source is used for the wafer exposure.[11] Therefore, the pitch 32nm horizontal dense LS is used as the wafer anchor, using mask CD 16nm to print wafer CD 16nm.

Figure 3 shows the CD-SEM images of the anchor feature both for the dry resist and the reference CAR, as well as the comparison of the measured Mask Error Enhancement Factor (MEEF) through pitches at the best dose and best focus condition. The MEEF is measured at the target CD equal to half pitch. There are slightly CD offsets for the wafer anchor of these two processes, however, our goal is to study and understand OPC model accuracy of the dry resist process; thus, we did not fine tune the exposure dose to print wafer CD 16nm on target. The measured MEEF through pitches on the right side of Fig. 3 indicates that dry resist delivers lower MEEF with respect to the reference CAR.
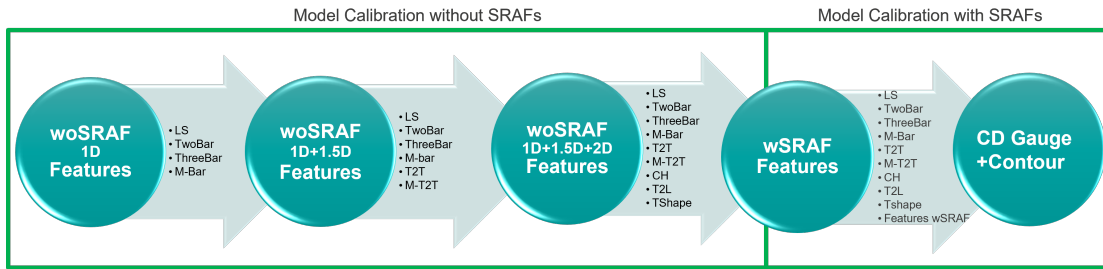
Figure 2: OPC modeling accuracy study strategy. The flow is divided into two parts, which contains five steps. All the 1D, 1.5D and 2D features are defined in Fig. 1. woSRAF: without SRAFs; wSRAF: with SRAF.
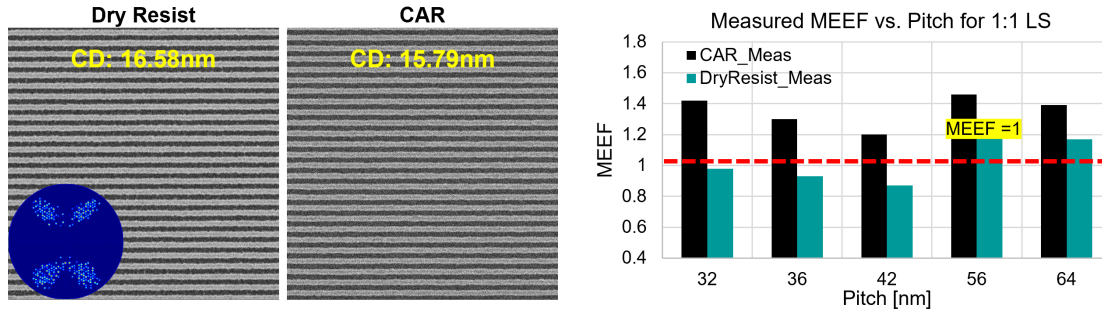

Figure 3: Anchor feature printability of the dry resist and the reference CAR, as well as the measured MEEF through pitches at the best dose and best focus condition. CAR: chemical amplified resist.

3.1 Mask Error Enhancement Factor

Figure 4 shows the impact of aerial image blur on the measured MEEF, aerial image blur is used to mimic the resist diffusion in the experiment. There is a slight difference on the wafer anchor of these two processes,
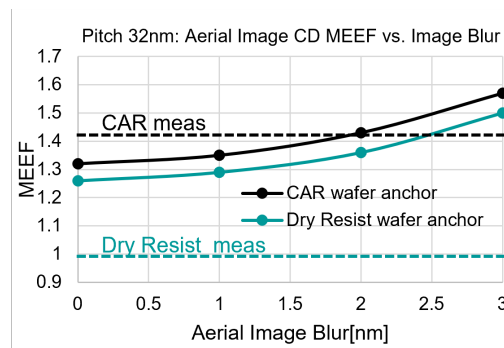

Figure 4: Aerial image blur impacts on the MEEF.

therefore, slightly different model thresholds are used in the simulation to mimic the experiment. The results indicate that the MEEF is becoming larger as the aerial image blur becomes larger. To match with the measured MEEF, 2nm aerial image blur is needed for the reference CAR, while the dry resist process performs lower MEEF than the aerial image CD MEEF (aerial image blur=0nm).
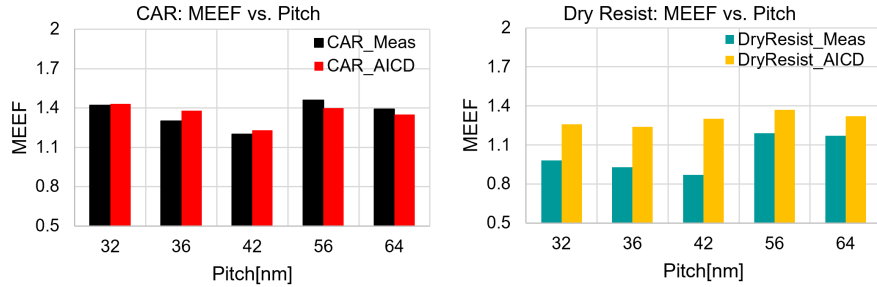
Figure 5: The measured MEEF with respect to the simulated aerial image CD MEEF. In the simulation, 2nm aerial image blur is used for the CAR, 0nm aerial image blur is used for the dry resist.

Figure 5 compares the measured MEEF with respect to the aerial image CD MEEF. In the simulation, 2nm aerial image blur is used for the reference CAR and 0nm aerial image blur is used for the dry resist, respectively. As shown in the figure, by using 2nm aerial image blur, the aerial image CD MEEF performs a good match with the measured MEEF of the reference CAR through pitches, while for the dry resist, there is a large deviation between the measured MEEF and simulated aerial image CD MEEF. The measured dry resist CD MEEF is lower than the aerial image CD MEEF through pitches.

3.2 Resist Shrink

Due to the dry development, dry resist has shown large resist film thickness loss for both blank resist and patterned resist, which can be up to 50%,[12] this effect might be due to the resist shrink. In calibre CM1, resist shrink terms have been developed to model resist shrink effect.[13] Figure 6 displays the model accuracy of 1D features without SRAFs, without using resist shrink terms and with resist shrink terms model error distributions are respectively shown on the left and the middle figures. As shown in these two figures, by using resist shrink terms, the model accuracy can be significantly reduced. The figure on the right side compares the model error trend with respect to the patterning density (CD/pitch) of the LS. Without using the shrink terms, model error is becoming larger as the pattern density becomes higher, and by using resist shrink terms, the model error trend can be completely removed.
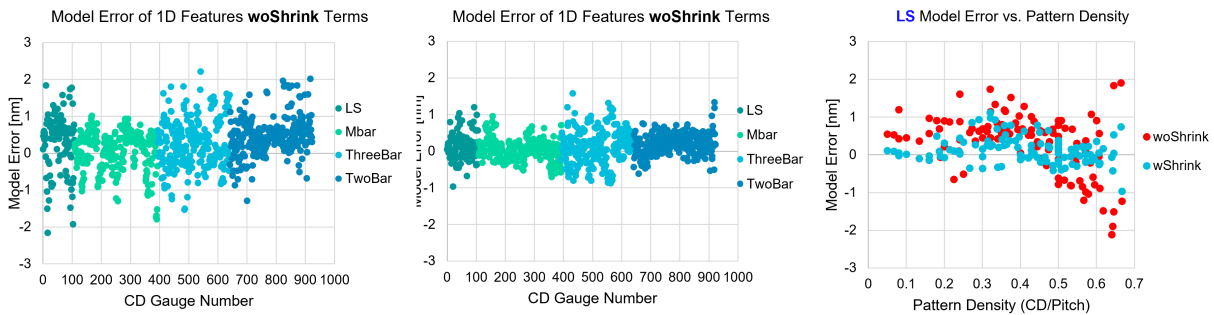

Figure 6: Model accuracy of 1D features (without SRAFs) without resist shrink terms vs. with resist shrink terms, as well as the model error trend with respect to the patterning density (CD/pitch) of the LS of the dry resist. (woShrink: without shrink; wShrink: with shrink.)

Figure 7 shows the comparison result of the measured MEEF and simulated MEEF. Without using resist shrink terms, the model can not capture the measured MEEF trend through pitches, and by using resist shrink terms, the model can accurately match the simulated MEEF to the measured MEEF.
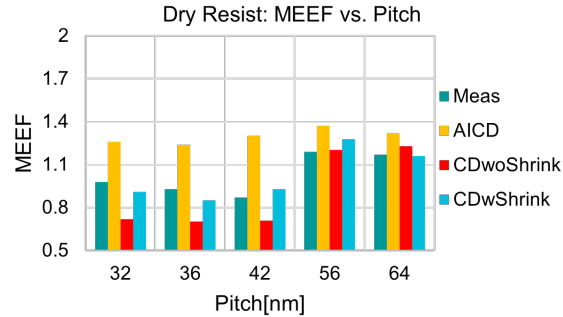
Figure 7: Measured and simulated MEEF through pitches. (Meas: Measured MEEF; AICD: aerial image CD MEEF with 0nm aerial image blur; CDwoShrink: resist model CD MEEF without shrink terms; CDwShrink: resist model CD MEEF with shrink terms.)

3.3 Proximity

Figure 8 illuminates the proximity curve through pitches at fixed mask CD 20nm for both CAR and dry resist, as well as the simulated aerial image CD and the wafer printability through pitches. For the reference CAR,
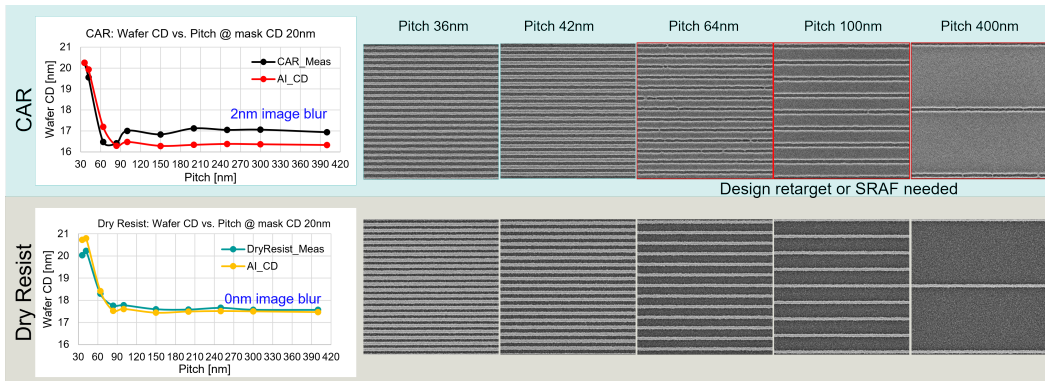

Figure 8: Proximity through pitches at fixed mask CD 20nm. (`AI_CD`: aerial image CD; 2nm aerial image blur is used for the CAR and 0nm aerial image is used for the dry resist during the simulation.)

the measured wafer CD has a good match with the aerial image CD (2nm aerial image blur is used) at smaller pitch, and there is a DC offset when the pitch becomes larger than 90nm. While for the dry resist, the measured wafer CD has a large deviation with respect to the aerial image CD at smaller pitch, and it starts to have a good match with the aerial image CD (0nm aerial image blur is used) when the pitch is larger than 90nm. The right side of the figure presents the wafer printability through pitches at fixed mask CD 20nm. For the reference CAR, the trench starts bridging for the semi-dense and isolated features, where design retarget or SRAF insertion is needed to guarantee good printability, while dry resist shows good printability through pitches.

3.4 Two-Bar and SRAF Printing

Figure 9 shows the printability of the Two-Bar at pitch 32nm. The bottom left figure is the aerial image profiles of the CAR (aerial image blur=2nm) and of the dry resist (aerial image blur=0nm), These two aerial image profiles are similar with slight difference (due to different aerial image blur applied). The middle column of the figure compares the printability of the Two-Bar. The reference CAR could not print horizontal pitch 32nm Two-Bar, while dry resist can deliver good printability of horizontal pitch 32nm Two-Bar with large process window (the right side of the figure shows the printability of pitch 32nm Two-Bar through dose and focus).
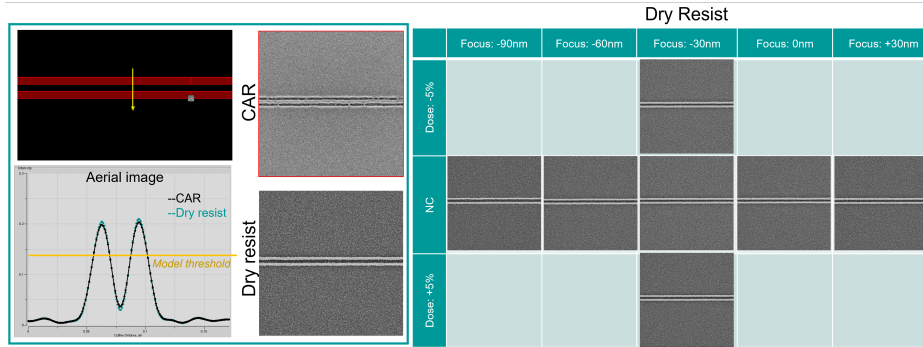
Figure 9: The printability of the Two-Bar at pitch 32nm without SRAF.

Considering the OPC of the fullchip design, SRAF insertion might be needed for some semi-isolated or isolated features. Figure 10 presents the pitch 32nm Two-Bar with SRAF, the SRAF CD is equal to 8nm. The aerial image profiles are very similar as well, however, SRAF printing behaviors are different on the wafer. The reference CAR could print pitch 32nm Two-Bar nicely, and no SRAF printing is observed, while dry resist shows SRAF printing issue, even though the maximum SRAF aerial image intensity is still far away to the model threshold. To understand this behavior, the image profiles are plotted on the right side of the figure. As shown in the figure, without resist shrink, the SRAF resist image intensity is far away to the model threshold, and there is no SRAF printing. By adding resist shrink terms, the SRAF resist image profile is enhanced, the max intensity touches the model threshold. The model with shrink terms can accurately capture the dry resist behaviors on the wafer. Therefore, the dry resist's sensitivity to SRAF printing is mainly due to resist shrink during dry development.
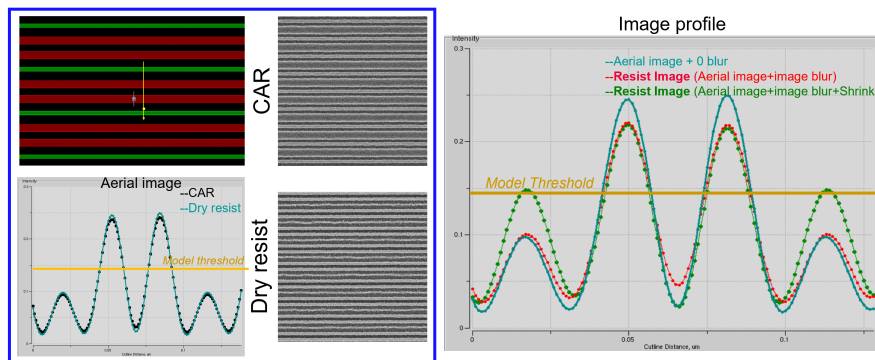

Figure 10: The printability of Two-Bar with SRAF, SRAF CD is equal to 8nm.

3.5 Tip-to-Tip Printing

Figure 11 displays the measured T2T CD with respect to the mask T2T CD at pitch 32nm, the mask CD is 16nm. The aerial image T2T CD curve is shown in the figure as well, where the 2nm aerial image blur is used for the CAR, and 0nm aerial image blur is used for the dry resist. The results demonstrate that there is a DC offset for the wafer T2T CD with respect to the aerial image T2T CD for the CAR, while dry resist wafer T2T CD has a good match with the simulated aerial image CD. The dry resist can print the wafer T2T CD 20nm with the mask T2T CD 13nm. For smaller mask T2T CD, the T2T bridging is observed on the wafer.

To study the T2T bridging, a new model is calibrated by using 1D and 1.5D features without SRAFs, the model error distribution is shown on the left side of Fig. 12. The right side of Fig. 12 shows the image profiles of T2T with the CD equal to 10nm and 13nm, respectively. As shown in the figure, with and without resist shrink terms, resist image profiles are similar. Thus, the resist shrink does not impact on the T2T printing, and
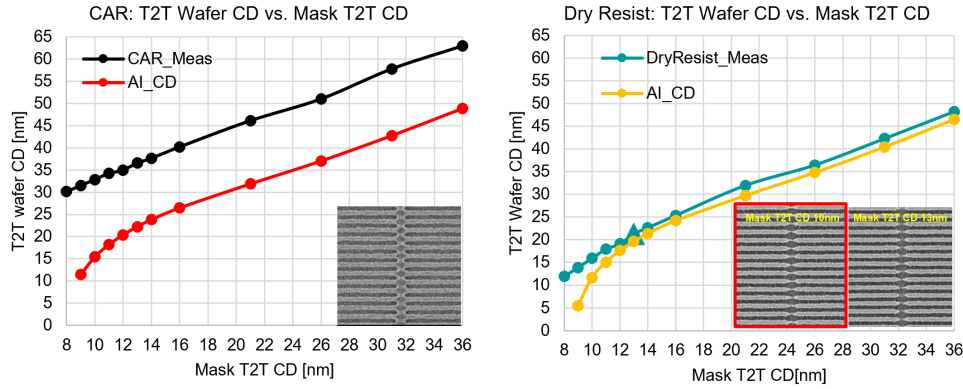
Figure 11: Measured wafer T2T CD with respect to the mask T2T CD at pitch 32nm, the mask CD is 16nm. (`AI_CD`: aerial image T2T CD, 2nm aerial image blur is used for the CAR, and 0nm aerial image blur is used for the dry resist.)

the T2T bridging at smaller mask T2T CD (10nm) is mainly due to the low aerial image contrast, which could not completely remove the resist at T2T.
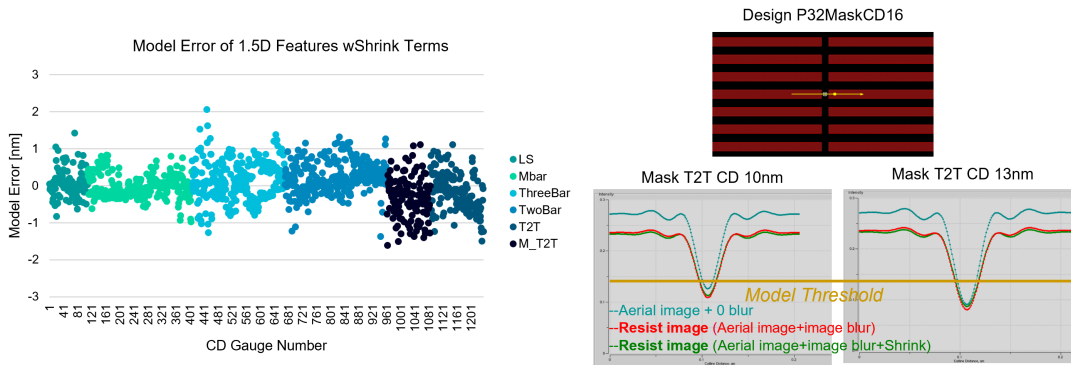

Figure 12: Model error distribution of 1D and 1.5D features without SRAF (left) and T2T image profiles comparison at mask T2T CD 10nm and 13nm (right). For the T2T comparison, the design is horizontal pitch 32nm with mask CD equal to 16nm.

4. SUMMARY

In this paper, we investigate the OPC model accuracy of dry resist process contacting on N5 design at k1=0.39. imec PoR CAR process is used as the reference. To have a good match with the optical model, dry resist requires less image diffusion, which means higher resolution for the lithographic patterning. Dry resist shows good proximity curve match between the wafer CD and aerial image CD for semi-iso and iso features, and SRAFs are not needed to print pitch 32nm Two-Bar. Due to the resist shrink during dry development, dry resist has lower MEEF than the CAR measured MEEF and is sensitive to the SRAF printing, which requires resist shrink terms in the CM1 model to capture the wafer CD trend. By using the resist shrink terms, CM1 model can accurately capture the dry resist printability on the wafer. Future work will focus on advanced modeling study and model error at advanced node will be reported.

ACKNOWLEDGMENTS

REFERENCES

[1] Levinson, H. J. and Brunner, T. A., "Current challenges and opportunities for EUV lithography," in [*International Conference on Extreme Ultraviolet Lithography 2018*], Ronse, K. G., Hendrickx, E., Naulleau, P. P., Gargini, P. A., and Itani, T., eds., **10809**, 5 – 11, International Society for Optics and Photonics, SPIE (2018).

[2] Meli, L., Petrillo, K., Silva, A. D., Arnold, J., Felix, N., Robinson, C., Briggs, B., Matham, S., Mignot, Y., Shearer, J., Hamieh, B., Hontake, K., Huli, L., Lemley, C., Hetzer, D., Liu, E., Akiteru, K., Kawakami, S., Shimoaoki, T., Hashimoto, Y., Ichinomiya, H., Kai, A., Tanaka, K., Jain, A., Choi, H., Saville, B., and Lenox, C., "Defect detection strategies and process partitioning for SE EUV patterning," in [*Extreme Ultraviolet (EUV) Lithography IX*], Goldberg, K. A., ed., **10583**, 87 – 103, International Society for Optics and Photonics, SPIE (2018).

[3] Simone, D. D., Rutigliani, V., Lorusso, G., Bisschop, P. D., Vesters, Y., Carballo, V. B., and Vandenberghe, G., "EUV photoresist patterning characterization for imec N7/N5 technology," in [*Extreme Ultraviolet (EUV) Lithography IX*], *Proc. SPIE* **10583**, 87 – 101 (2018).

[4] Bisschop, P. D. and Hendrickx, E., "Stochastic printing failures in EUV lithography," in [*Extreme Ultraviolet (EUV) Lithography X*], Goldberg, K. A., ed., **10957**, 37 – 56, International Society for Optics and Photonics, SPIE (2019).

[5] Gallatin, G. M., "Resist blur and line edge roughness," in [*Optical Microlithography XVIII*], *Proc. SPIE* **5754**, 38 – 52 (2005).

[6] Steenwinckel, D. V., Gronheid, R., Lammers, J. H., Meyers, A. M., Roey, F. V., and Willems, P., "A novel method for characterizing resist performance," in [*Advances in Resist Materials and Processing Technology XXIV*], Lin, Q., ed., **6519**, 65190V, International Society for Optics and Photonics, SPIE (2007).

[7] Bristol, R. L., "The tri-lateral challenge of resolution, photospeed, and LER: scaling below 50nm?," in [*Advances in Resist Materials and Processing Technology XXIV*], Lin, Q., ed., **6519**, 65190W, International Society for Optics and Photonics, SPIE (2007).

[8] Alvi, M., Gottscho, R., Haider, A., Heo, S., Hsieh, P., Huang, C.-C., Jurczak, G., Kam, B., Kim, J. Y., Li, B., Li, D., Nguyen, H., Pan, Y., Peter, D., Shamma, N., Silva, A. D., Tan, S., Wang, E., Weidman, T., Wise, R., Wu, M., Verveniotis, E., Volosskiy, B., Yu, J., and Zaid, H., "Achieving zero EUV patterning defect with dry photoresist system," in [*Advances in Patterning Materials and Processes XXXIX*], Sanders, D. P. and Guerrero, D., eds., **PC12055**, PC120550B, International Society for Optics and Photonics, SPIE (2022).

[9] Wise, R. S., "Breaking stochastic tradeoffs with a dry deposited and dry developed EUV photoresist system," in [*Advances in Patterning Materials and Processes XXXVIII*], Sanders, D. P. and Guerrero, D., eds., **11612**, 1161203, International Society for Optics and Photonics, SPIE (2021).

[10] Suh, H. S., Simone, D. D., Beral, C., Gupta, M., Vandenbroeck, N., Silva, A. D., Haider, A., Huang, C.-C., Brouri, M., Gullo, F., Jambaldinni, S., Kam, B., Zaid, H., Verveniotis, E., Tan, S., Weidman, T., Yu, J., Li, D., Xue, J., and Lee, Y., "Dry resist patterning readiness towards high-NA EUV lithography," in [*Advances in Patterning Materials and Processes XL*], Guerrero, D. and Amblard, G. R., eds., **12498**, 1249803, International Society for Optics and Photonics, SPIE (2023).

[11] Rio, D., Blanco, V., Franke, J.-H., Gillijns, W., Dusa, M., Poortere, E. D., Adrichem, P. V., Lyakhova, K., Spence, C., Hendrickx, E., Biesemans, S., and Nafus, K., "EUV pupil optimization for 32nm pitch logic structures," in [*International Conference on Extreme Ultraviolet Lithography 2018*], Ronse, K. G., Hendrickx, E., Naulleau, P. P., Gargini, P. A., and Itani, T., eds., **10809**, 104 – 117, International Society for Optics and Photonics, SPIE (2018).

[12] Lorusso, G. F., Heuvel, D. V. D., Zidan, M., Moussa, A., Beral, C., Charley, A.-L., Simone, D. D., Silva, A. D., Verveniotis, E., Haider, A., Kondo, T., Shindo, H., Ebizuka, Y., and Isawa, M., "Dry resist metrology readiness for high-NA EUVL," in [*Metrology, Inspection, and Process Control XXXVII*], Robinson, J. C. and Sendelbach, M. J., eds., **12496**, 1249612, International Society for Optics and Photonics, SPIE (2023).

[13] Granik, Y., "Analytical solutions for the deformation of a photoresist film," in [*Optical Microlithography XXXII*], Kye, J. and Owa, S., eds., **10961**, 109610D, International Society for Optics and Photonics, SPIE (2019).